Thermodynamics Control Reactivity of Hypervalent Iodine-Mediated Styrene Hetero- and Homodimerization: Mechanistic Insights

Aqeel A. Hussein,[1,2] * Ahmed Al-Yasari [3,4] and Yumaio Ma[5]

[1] School of Chemistry, University of Southampton, Southampton, Hampshire, SO17 1BJ, United Kingdom.

[2] College of Dentistry, University of Al-Ameed, Karbala PO Box 198, Iraq.

[3] School of Chemistry, University of East Anglia, Norwich, NR4 7TJ, United Kingdom.

[4] Department of Chemistry, Faculty of Sciences, University of Kerbala, Kerbala, Iraq.

[5] BSJ Institute, Haidian, Beijing, 100084, People's Republic of China.

*Email: aahh1f19@soton.ac.uk

Abstract

A mechanistic insight into the hetero- and homodimerizations (HETD and HOMD) of styrenes promoted by hypervalent iodine reagents (HVIRs; **DMP** and **PIDA**) and facilitated by HFIP to yield all *trans* cyclobutanes is reported using density functional theory (DFT) calculations. The HFIP molecules lower the energy of the single electron oxidation (SEO) or initiation as a result of strong hydrogen bonding interactions that substantially stabilize the frontier orbitals before and after electron addition. The HETD or HOMD is a radically-characterized π-π stacked head-to-head stepwise [2+2] cycloaddition initiated via SEO by **DMP** or **PIDA**, respectively. DFT results supported by quasiclassical molecular dynamics simulations show that HOMD is a competing pathway to HETD although the latter is relatively faster, in accordance with experimental observations. The initiation is a rate-determining step as a thermodynamically endergonic and propagation is accomplished by radically-cationic hetero- and homodimerized intermediate as propagation is faster than single electron reduction (SER) or termination by radically-anionic HVIRs. Initiation by **DMP** found to be faster and less endergonic than by **PIDA** due to (1) the energy gap of electron transfer in a SEO step by I(V) is lower than I(III) and (2) the SOMO energy of the radical anion I(V) is lower than I(III). Furthermore, the presence of *p*-methoxy group is essential to underpin the SEO by which the more thermodynamically favorable SEO leads to a successful cycloaddition as the thermodynamic term represents a major contribution in the initiative barrier.

Introduction

Stereoselective approaches to substituted cyclobutanes have been captivated by organic chemists to be of high interest despite of its challenging requirements.[1, 2] Due to the fact that these cyclobutane rings exist in many bioactive natural products (Figure 1-a),[3-5] the need for such efficient, reliable, and benign synthesis methods is

still under developing strategies to get a purely chiral strained carbocycle. Regardless the many different synthetic methodologies appeared in literatures to access cyclobutanes,[6-11] the olefin dimerization via oxidative manners, which involves an active radical cation intermediate formation, represents a helpful and promising tactic to reach. The olefin dimerization was firstly reported by Ledwith[12, 13] and Bauld,[14-16]. In this regard, metal complexes[17] and organic [18, 19] photoredox catalysis have been applied to promote such a nice cyclization.[20-28] Recently, a major contribution to this field has been exploited by using catalytic amounts of HVIR [29, 30] in HFIP to investigate a stereoselective functionalization of alkenes.[31-33] The HFIP has been shown to be a unique solvent due its significant role of hydrogen bonding [34-36] that enables the HVIR to act as single electron oxidants.[37-40] Based on the utility of the HVIR/HFIP, Donohoe and co-workers have developed a diastereoselective [2+2] cycloaddition of alkenes with remarkable results (Figure 1-b).[41, 42] The mechanism proposed involves a SEO of styrene **1** to a radical cation **1+** by HVIR followed by either HOMD, where dimerization proceeds with another molecule of styrene **1** in the presence of I(III) **PIDA**, or HETD, where dimerization proceeds with a different alkene **2** in the presence of I(V) **DMP**, to give the all *trans* cyclobutane product **3** after the re-addition of an electron to the product.

a) Bioactive natural products:



Nigramide R   ζ-Truxinanilide
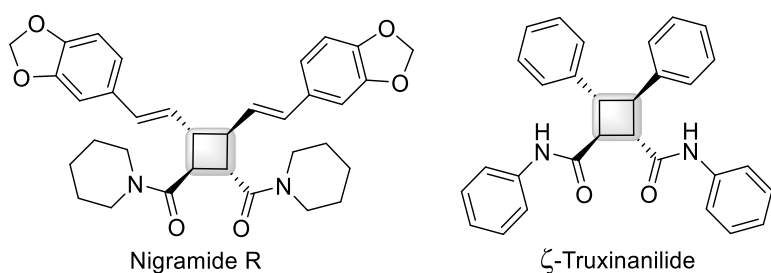
b) Iodine-mediated dimerization of Styrenes:
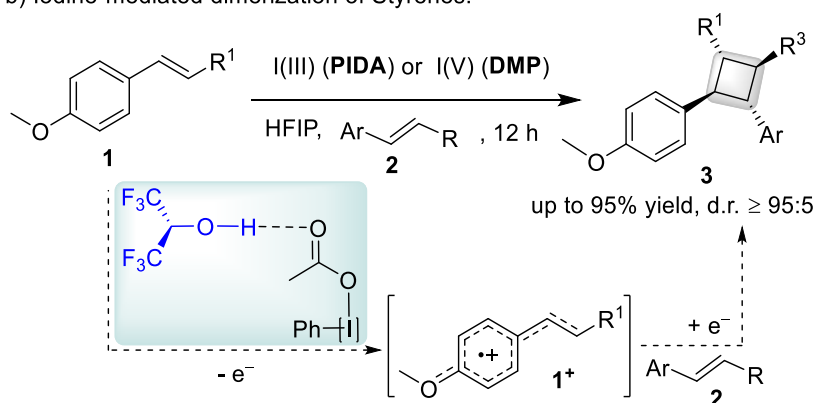
Figure 1. a) Examples of bioactive natural products containing cyclobutane ring. b) HOMD or HETD of styrenes with phenyliodine(III) diacetate (**PIDA**) or Dess-Martin periodinane (**DMP**), respectively .

The existence of hydrogen bonding interactions between the HFIP and **PIDA** has been proposed to be essential and the physical origin of the enhanced oxidative strength for the iodine reagent.[43] In addition to the almost disappearance of HO signals from NMR experiments, the voltammetric peak potential experiments measured versus Fc/Fc+ demonstrated a shift in reduction potentials for **PIDA** ($E_{p,c}$ in ACN = −1.32 V, $E_{p,c}$ in HFIP =

−0.47 V). The possibility of ligand exchange between HFIP and **PIDA** has been excluded and any altered reactivity to the oxidants is ruled out as the HFIP is a low nucleophilic solvent.[43-47] All of the above-mentioned study concerns the first step of the reaction, the SEO step, and seems to us in need for further understandings, however, the subsequent steps that lead to the all *trans* cyclobutane ring are not considered, at least to the best of our knowledge, by other workers under these conditions.[26, 48-50] At this point, the reaction mechanism and reactivity of HVIR-mediate dimerization exclusively appears incomplete and warrants further attentions (Figure 2).. Therefore, we herein interpret DFT simulations on the HOMD and HETD that gives all *trans* cyclobutane under HVIRs with **PIDA** and **DMP**, respectively, featuring (1) the effect of HFIP on reactivity of this protocol, (2) the competition between the unwanted termination and propagations, (3) realizing the competition between homo- and heterodimerization via potential energy surfaces (PES) and quasiclassical trajectory molecular dynamics (QCTMD) simulations, (4) nature of cycloaddition, and (5) reactivities and stabilities of the correspondent charged radicals formed in this synthetic utility.
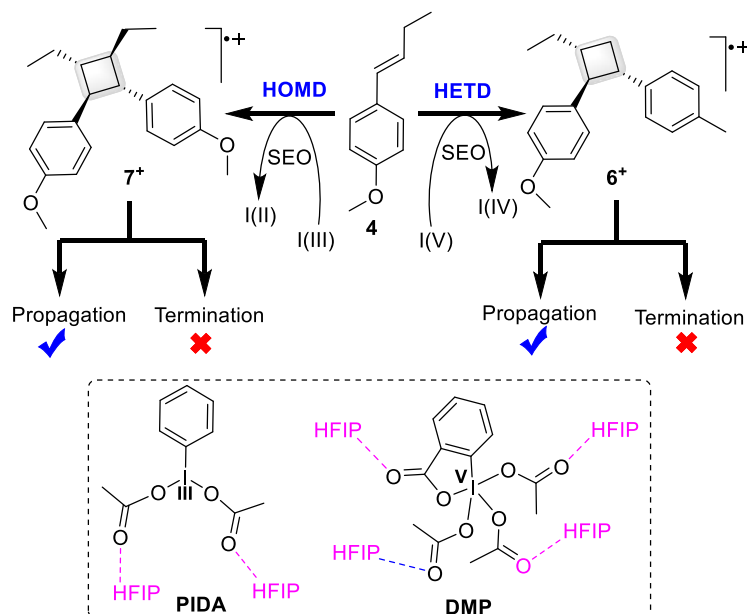
Figure 2. General representation of the HVIR [2+2] cycloaddition considered in this study, where iodine reagents are hydrogen bonded to HFIP explicitly.

Results and Discussion

To explore our HVIR-mediated dimerization of styrenes, we have divided our discussions into five distinct sections with the following order: validation of our strategy, mechanism of dimerization, competition between HOMD and HETD, and stability of the SEO and effect of substituents on SEO.

Validation of strategy and level of theory

The calculations were conducted in explicit and implicit HFIP. The explicit HFIP protocol means that every single acetate groups in **PIDA** and **DMP** is hydrogen bonded to one HFIP molecule to match the experimental

conditions, whereas the implicit protocol is performed only with continuum solvation model based on density (IEFPCM-SMD). All structures were initially calculated using the wB97XD/6-311+G(d,p)/LANL2DZ//6-31G(d)/LANL2DZ level of theory, however we found inconsistencies with the experimental results because of Fe and I atoms. Therefore, we carried out a basis set search on Fe and I atoms through running single point energy calculations on optimized structure by 6-31G(d)/LANL2DZ through comparison between measured and calculated voltammetric peak potentials for redox species of different substituted *trans-β*-methylstyrenes toward **PIDA** (Figure 10, see below). For Fc/Fc$^+$, as shown in ESI, the cyclopentadienyl group in Fc was tested with a basis set of triple- ζ quality (6-31G(d,p)) to be consistent with the valence basis sets used for iron. We found that Def2-TZVPP/6-31G(d,p) level of theory gives the best agreement with the experimental redox potential values of different substituted *trans-β*-methylstyrenes using Cp$_2$Fe (calculated $E^{1/2}$ = 4.84 V) as reference to calculate their redox potentials (see Figure 10). For iodine in **PIDA**, it was found that the basis set Def2-TZVPP for iodine and 6-311+G(d,p) for C, H, and O atoms gave the best agreement with experimental redox potentials (see ESI). Importantly, and under explicit protocol, the calculated value for **PIDA$_{HFIP}$** + e$^-$ → **PIDA$^-_{HFIP}$** is $E^{1/2}$ = 4.25 V of peak potential for **PIDA$_{HFIP}$** is $E_{p,c}$ = −0.59 V versus calculated peak potential Fc/Fc$^+$ ($E^{1/2}$ = 4.84 V) as a reference, leading to a good agreement with the measured peak potential for **PIDA** is $E_{p,c}$ = −0.47 V. Under implicit protocol, the calculated value of non-hydrogen-bonded **PIDA** is $E^{1/2}$ = 4.02 V of peak potential $E_{p,c}$ = −0.82 V versus Fc/Fc$^+$ with a shifting to more negative value of 230 mV less favorable than explicit **PIDA$_{HFIP}$**. Using this strategy, a good agreement between the measured and calculated peak potential have been achieved as shown in Figure 10. Therefore, the wB97XD/def2-TZVPP/6-311+G(d) level of theory is used for oxidants whereas the wB97XD/def2-TZVPP/6-31G(d,p) level of theory is utilized for Cp$_2$Fe in order to calculate the redox potentials.

Mechanism of dimerization

Our DFT investigations with the exploration of the HETD and HOMD facilitated by **DMP** and **PIDA**, respectively, are considered. The cyclobutane ring formation is investigated based on the SEO and single electron reduction (SER). When the SEO and SER are initiated and terminated, respectively, through only HVIR to get cyclobutane ring formed, this is a catalytic mechanism. The more plausible scenario is that the HVIR only initiates the reaction to get the styrene molecule radicalized by SEO and propagation of the reaction proceeds without HVIR and this is an initiated or propagated mechanism as the HVIR serves as an initiator.

To account better knowledge about the height barrier of SEO, free energy of activation for the SEO was calculated using four-point method proposed by Nelsen (see ESI).[51-53] We are convinced that this method result in a reasonable estimation of the electron transfer (ET) activation barrier.

It has been reported that HFIP plays a critical role with oxidizing agent rather than with the radical cation formed.[43] The effect of explicit hydrogen bonding in our calculations is considered only on the SEO steps, namely the first and fourth reaction step (FRS and FoRS, respectively, as shown in Figure 3 and 4), whereas the cyclization steps, namely the second and third reaction steps (SRS and TRS, respectively, as shown in Figure 3 and 4), are proceeded with an implicit HFIP protocol.

HETD pathway. The DFT results of HETD in the presence I(V) **DMP** with and without explicit HFIP molecules are shown in Figure 3. Generally, the explicit HFIP molecule decreases the overall energetic pathway for the HETD over the nonexplicit one due to the hydrogen bonding between DMP and HFIP which agrees with the findings of Donohoe and co-workers. The decrease is around 5 kcal mol^{-1} for the SEO step, FRS, and SER step, FoRS, and more than 6 kcal mol^{-1} for SRS and TRS. In the presence of explicit HFIP the free energy of activation for SEO for the FRS was found to be 20.2 kcal mol^{-1} to give radical cation **4$^+$** and radical anion **DMP$^-$$_{HFIP}$** as an endergonic step (ΔG_r = 13.8 kcal mol^{-1}). In absence of explicit HIFP the barrier for SEO increased to 25.4 kcal mol^{-1} as a more endergonic process (ΔG_r = 21.8 kcal mol^{-1}). An apparent increased in the I–O bond distances, clearly represented for the perpendicular acetate units to the phenyl iodine. After the ET, the I–O bond distances elongate from 2.08 and 2.15 Å to 2.63 Å and 2.99 Å when HFIP are not involved in calculations explicitly (see **DMP** and **DMP$^-$** in Figure 3). Elongation is slightly less when HFIP is involved explicitly, where I–O bond length is 2.12 Å is before the SEO and 2.55 Å and 2.77 Å are after the SEO (see **DMP$_{HFIP}$** and **DMP$^-$$_{HFIP}$** in Figure 5-a). The increase in distance is reasonably attributed to the repulsions with the single unpaired electron existed on iodine (see spin density contours below).

All PES trails to find a concerted [2+2] cycloaddition TS for the cation cyclobutane formation **6$^+$** are unsuccessful and, therefore, a two-step mechanism have been taken through the SRS and TRS. For the SRS, the head-to-head first C–C bond formation was found to have a barrier of 8.3 kcal mol^{-1} via TS **8$^+$** with bond length of 2.20 Å along the TS is established, giving uncyclized intermediate **9$^+$** with C–C bond being formed at 1.58 Å as a thermoneutral step of 0.1 kcal mol^{-1} (Figure 3).[54] The TS **8$^+$** shows a π-π stacking interaction of 3.6 Å. A higher barrier TS of 13.1 kcal mol^{-1} was found without π-π stacking (see Figure S2 in ESI). It seems that the favorable π-π stacking plays an important role in controlling the configurations of the product to be all *trans* cyclobutane. The presence of non-covalent interaction, π-π stacking, for TS **8$^+$** and intermediate **9$^+$** is shown by Reduced Density Gradient (RDG) analysis (Figure 5-c).[55] Attractive π-π interaction is clearly seen in the green areas between the two phenyl rings. The nature of interaction between **4$^+$** and **5** through TS **8$^+$** has a radical character due to SOMO-HOMO overlapping. The SOMO orbitals located on radical styrene **4$^+$** is overlapped with the HOMOs of **5** with an energy gap if 4.03 eV (see Figure S6). The radical cation intermediate **9$^+$** cyclizes to the cationic cyclobutane **6$^+$**, the TRS, in a low barrier step of $\Delta G^\ddagger$ = 7.1 kcal mol^{-1} with a long C—C bond of 2.74 Å along TS **10$^+$** but in a slightly exergonic step (ΔG_r = −2.1 kcal mol^{-1}). Noticeably, the new C–C bond formed in cyclobutane **6$^+$** is 1.64 Å whereas all other C–C bonds in the ring are 1.54 Å, and this is attributed to radical character as indicated by the partial delocalization shown by spin density and β-LUMO contours (see Figure S8).

To release the cyclobutane **6**, the radical cation **6$^+$** undergoes SER by either the radical anion **DMP$^-$$_{HFIP}$** or another styrene to propagate the reaction. The SER step to cyclobutane cation **6$^+$** by **DMP$^-$$_{HFIP}$** needs a barrier of 4.3 kcal mol^{-1} as an exergonic step (ΔG_r = −20.4 kcal mol^{-1}) (Figure 3). If this is true, the reaction would need longer time to complete as the reaction will need an initiation of higher energy step (FRS) in every single cyclobutane formation. Thus, propagation through oxidation of another styrene **4** by **6$^+$** is more favored. The

oxidation of styrene **4** by **6⁺** is nearly to be barrierless of 1.1 kcal mol⁻¹ as an exergonic step ($\Delta G_r = -6.6$ kcal mol⁻¹) (Figure 6).
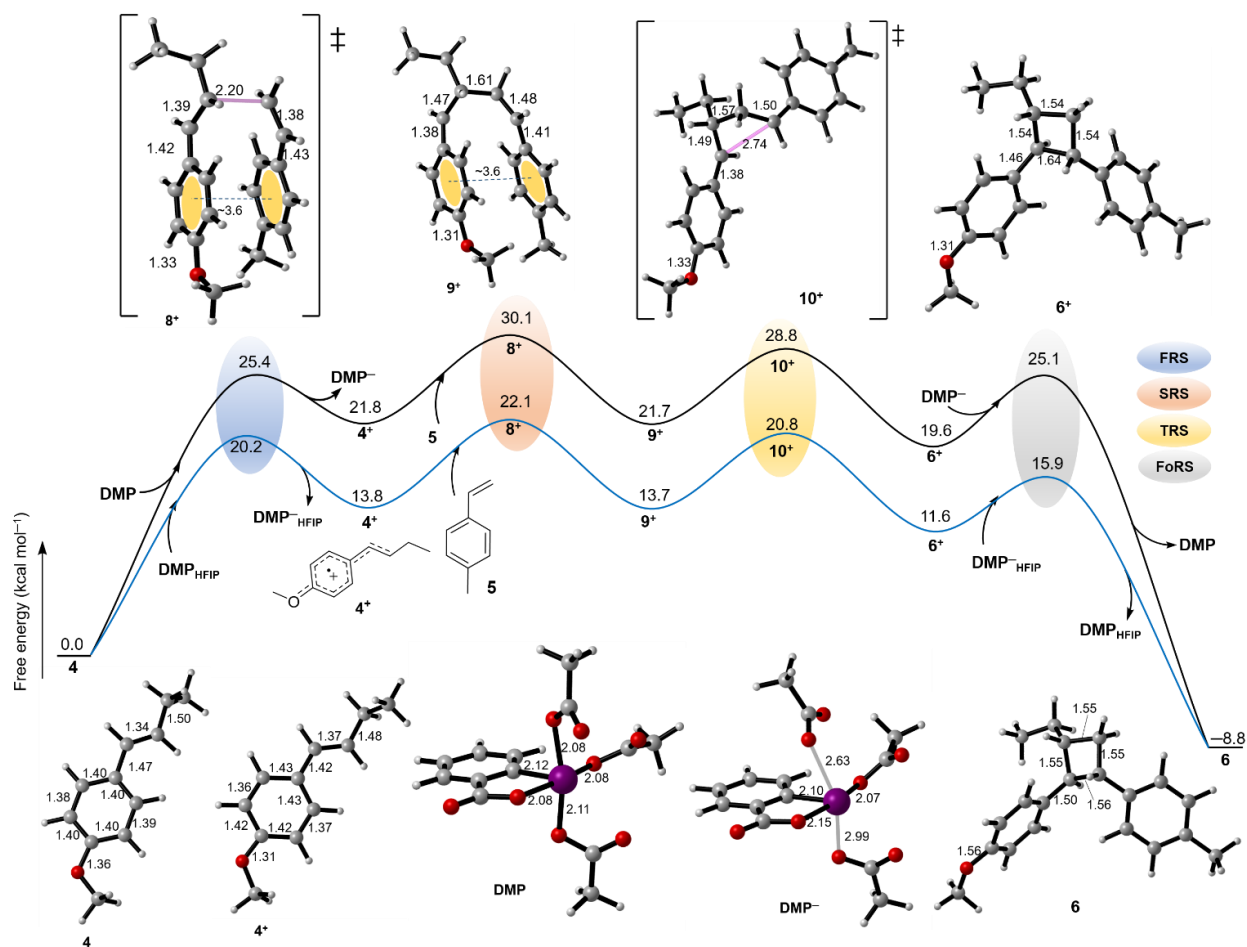
Figure 3. Free energy profile for the catalytic mechanism of **DMP**-mediated heterodimerization of styrenes (**4**) and (**5**), where SEO and SER proceed through only **DMP** to get cyclobutane ring formed, with explicit HFIP (blue pathway) and implicit HFIP (black pathway). Structures of **DMP**$_{HFIP}$ and **DMP⁻**$_{HFIP}$ are shown in Figure 5-a. The FRS and FoRS are the first and fourth reaction step for the SEO and SER steps, respectively, and their barriers were estimated based on Nelsen four-point method explained in SI. The SRS and TRS are the second and third reaction steps showing the first and second C−C bond formation.

HOMD pathway. Following the same strategy for HETD, the HOMD mechanism in the presence I(III) **PIDA** with and without explicit HFIP molecules is investigated and shown in Figure 4. As shown above with HETD, the explicit HFIP pathway shows lower energetic level than the nonexplicit pathway. The barrier of SEO, the FRS, was found to be 31.3 kcal mol⁻¹ to give radical cation **4⁺** and anion **PIDA⁻**$_{HFIP}$ as an endergonic step ($\Delta G_r = 28.1$ kcal mol⁻¹). The SEO for HOMD is more endergonic than for the HETD. The calculated endergonicity for initiation by **PIDA**$_{HFIP}$ is in excellent agreement with that measured for *trans* anethol **14** (see Figure 10).[43] Following the SEO step the bond length of the acetate group to iodine, namely I–O bonds, increases from 2.15 Å to around 2.58 Å for the non-hydrogen bonded **PIDA** (Figure 4) and to longer distances of 2.66 Å and 2.78 Å for the hydrogen-bonded one **PIDA**$_{HFIP}$ (Figure 5-b) for the reason mentioned above for SEO by **DMP**$_{HFIP}$.
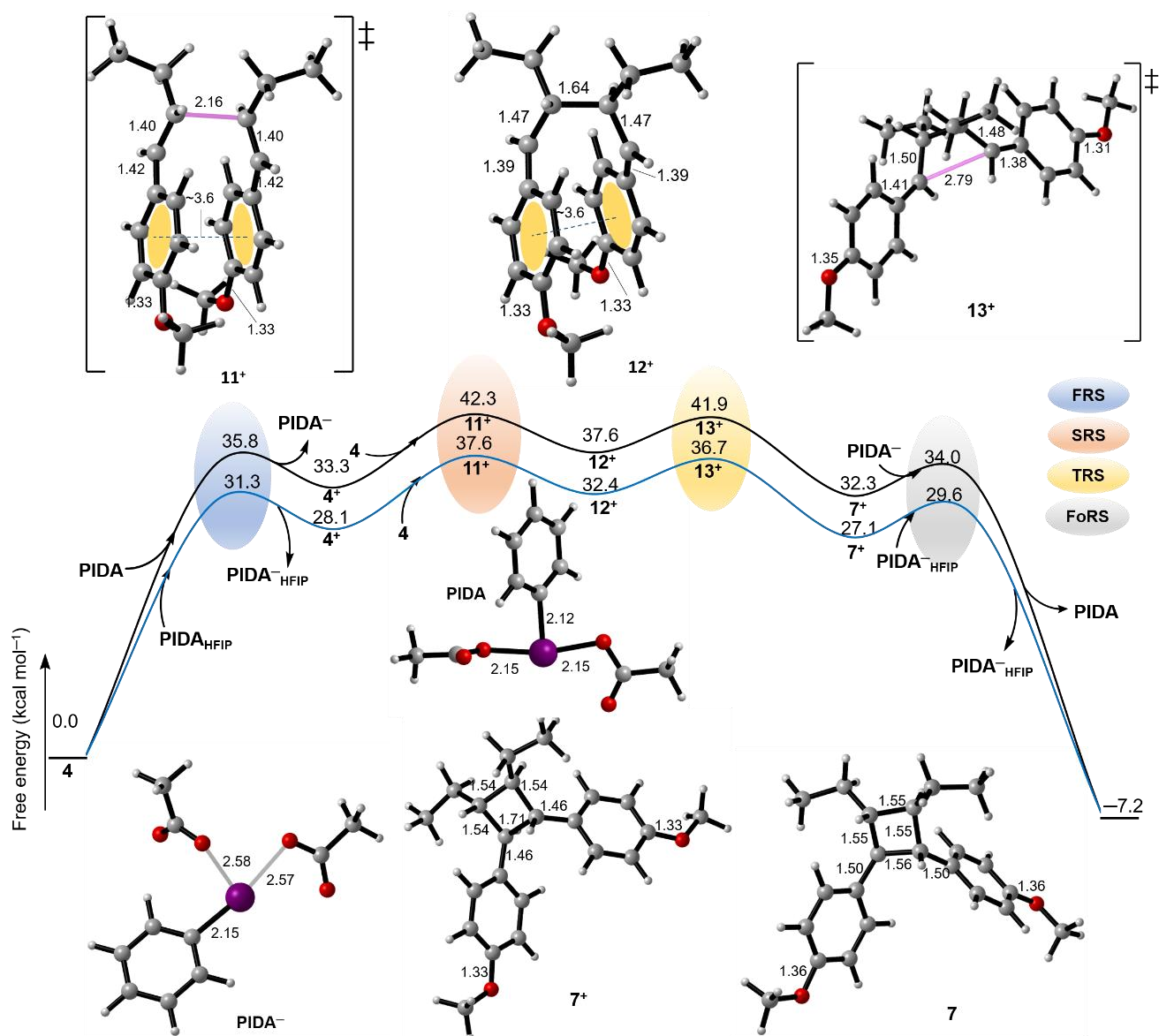
Figure 4. Free energy profile for the catalytic mechanism of **PIDA**-mediated homodimerization of styrenes (**4**), where SEO and SER proceed through only **PIDA** to get cyclobutane ring formed, with explicit HFIP (blue pathway) and implicit HFIP (black pathway). Structures of **PIDA_HFIP** and **PIDA⁻_HFIP** are shown in Figure 5-b. The FRS and FoRS are the first and fourth reaction step for the SEO and SER steps, respectively, and their barriers were estimated based on Nelsen four-point method explained in ESI. The SRS and TRS are the second and third reaction steps showing the first and second C−C bond formation.

The process for $\mathbf{4^+} \rightarrow \mathbf{12^+}$, the SRS, has a reasonable barrier of 9.5 kcal mol⁻¹ via π-π stacked head-to-head TS **11⁺** with bond length of 2.16 Å to give the cationic uncyclized intermediate **12⁺** as an endergonic step of 4.3 kcal mol⁻¹.[54] The favorable non-covalent interaction that represents the π-π stacking interaction between the two phenyl rings is shown in Figure 5-d. A higher barrier TS of 12.9 kcal mol⁻¹ was found for the first C-C bond formation when aromatic rings are not stacked (Figure S2). Likely to TS **8⁺**, TS **11⁺** has a radical character with an energy gap of 4.86 eV (see Figure S7) which is higher than for the HETD (**4⁺** and **5**). The first C–C bond

formation in 12^+ is longer than for that found for the uncyclized heterodimerized intermediate 9^+. The cyclization, TRS, is a low barrier step of 4.3 kcal mol^{-1} through TS 13^+ with C—C bond at 2.16 Å is seen to give the cationic homodimerized cyclobutane 7^+ as an exergonic step ($12^+ \rightarrow 7^+$, $\Delta G_r = -5.3$ kcal mol^{-1}). Upon formation of 7^+, the unpaired electron has totally delocalized over the entire system of 7^+ (see Figure S8) and resulted in an increase in the new C–C bond to be 1.71 Å, being longer than for 6^+.
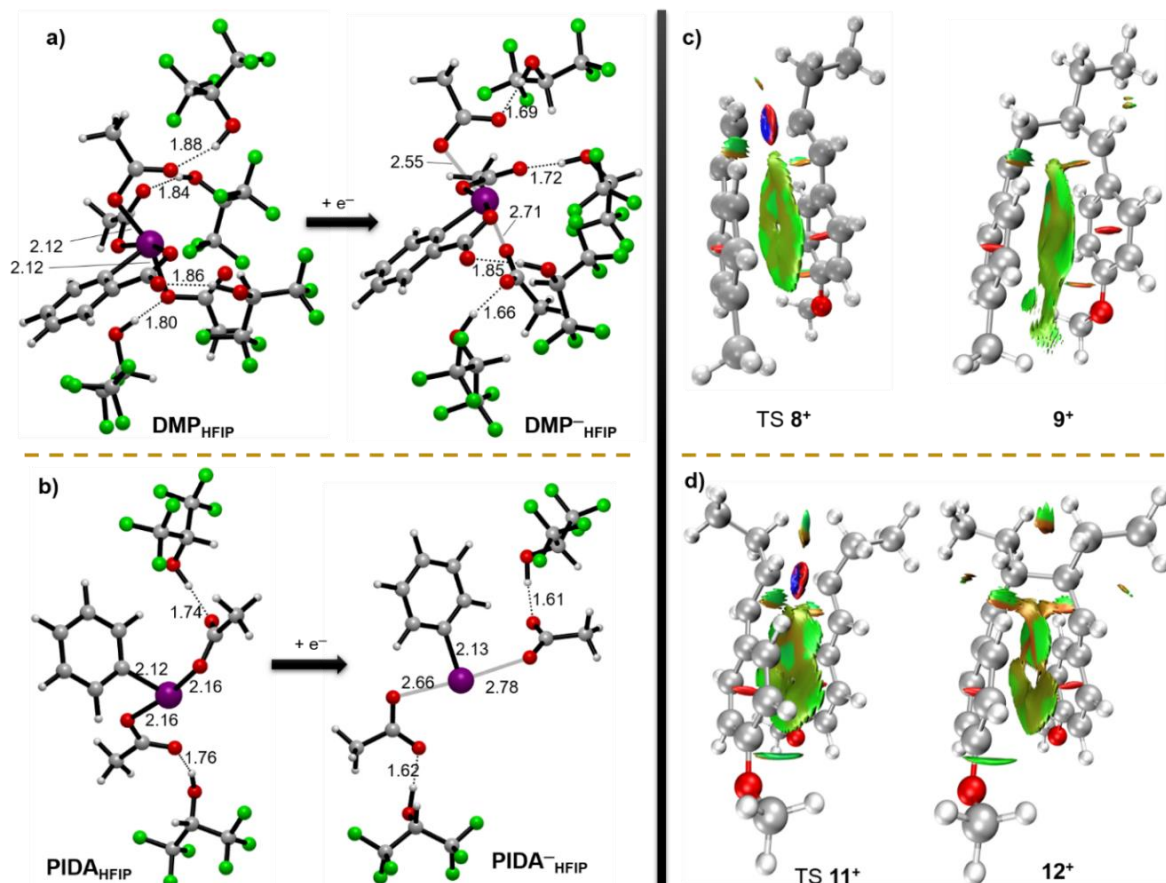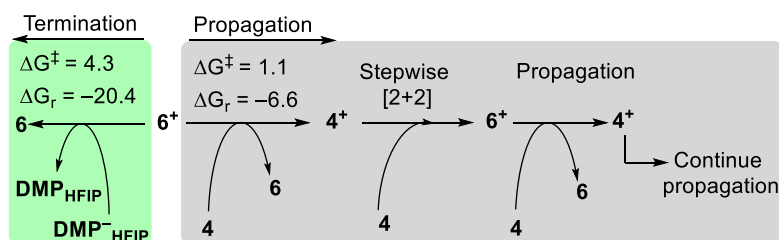

Figure 5. (a) and (b)Optimized hydrogen-bonded neutral and anion species of **DMP**$_{HFIP}$ and **PIDA**$_{HFIP}$. (c) and (d) Reduced Density Gradient (RDG) isosurface (isovalue at 0.5) for TSs 8^+ and 11^+ and intermediates 9^+ and 12^+, where attractive π-π stacking interactions are shown in green area, whereas red and blue area indicates steric repulsion and strong interactions, respectively.

The release of neutral homodimerized cyclobutane **7** via propagation process (Figure 6) is calculated to be favored over SER by radical anion **PIDA**$^-$$_{HFIP}$ (Figure 4). The oxidation of styrene **4** by 7^+ is found to be nearly barrierless of 1.5 kcal mol^{-1} as an exergonic step ($\Delta G_r = -6.3$ kcal mol^{-1}) (Figure 6). The SER by **PIDA**$^-$$_{HFIP}$ requires higher barrier of 2.5 kcal mol^{-1} as a result of the high exergonicity ($\Delta G_r = -34.4$ kcal mol^{-1}) needed to release the neutral cyclobutane **7** (Figure 4). This would indicate that reorganization energy plays an important role in driving the reaction toward propagation over termination by radical anionic HVIR. Overall, this would mean that the reaction is only initiated by the **DMP** or **PIDA** reagents and a very low concentration of radical cation 4^+ might be enough to reach the HETD or HOMD completed.

a) HETD

Termination | Propagation

Termination

$\Delta G^\ddagger = 4.3$
$\Delta G_r = -20.4$
6 ← **6⁺**

DMPHFIP
DMP⁻HFIP

Propagation

$\Delta G^\ddagger = 1.1$
$\Delta G_r = -6.6$
4⁺   Stepwise [2+2]   **6⁺**   Propagation   **4⁺**

6   **6**

4   **4**   **4**   → Continue propagation

b) HOMD

Termination | Propagation

Termination

$\Delta G^\ddagger = 2.5$
$\Delta G_r = -34.4$
7 ← **7⁺**

PIDAHFIP
PIDA⁻HFIP

Propagation

$\Delta G^\ddagger = 1.5$
$\Delta G_r = -6.3$
4⁺   Stepwise [2+2]   **7⁺**   Propagation   **4⁺**

7   **7**

**4**   **4**   **4**   → Continue propagation
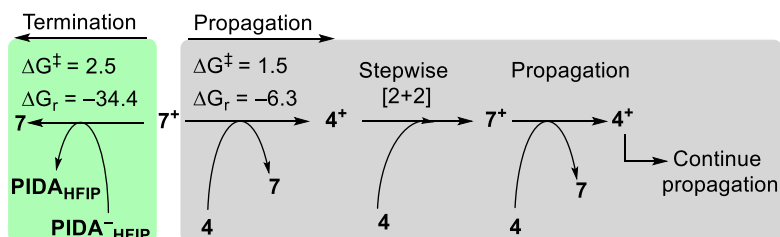
Figure 6. Propagation of HOMD and HETD.

Competition between HETD and HOMD

In general, the initiative SEO step from styrene **4** is shown to be more reactive with **DMP** catalyst since the SEO occurs with the more deficient catalyst I(V) (LUMO = −1.56 eV) over less deficient one I(III) (LUMO = −0.73 eV), apparently indicating that the initiation in HETD is faster than HOMD under **DMP** conditions. However, and from a synthetically perspective point of view, there is a competition between both processes which is experimentally seen. This concerns the fact that HOMD can relatively be accessed via HETD conditions. Our simulations have recognized these complications and shown to be problematic after initiation, FRS, takes place via I(V) catalyst (**DMP**HFIP). The calculations indicate that once the radical cation **4⁺** is formed, entering homo [2+2] cycloaddition is competitive. The results above (Figure 3 and 4) reveal that the HOMD starts with a barrier of 9.5 kcal mol⁻¹ via TS **11⁺** whereas HETD starts with lower barriers of 8.3 kcal mol⁻¹ via TS **8⁺**, implying difference between HOMD and HETD to be $\Delta\Delta G^\ddagger = 1.2$ kcal mol⁻¹. This is in general good agreement with the experimental findings, in which the HETD reaction proceeds an equivalent ratio of styrenes **5** to **4** of 2:1.[41] A further evidence for the competition between HOMD and HETD is emerged form QCT molecular dynamics of the first C–C bond formation (shown below).

Quasiclassical trajectory molecular dynamics (QCTMD) calculations. QCTMD simulations were utilized to understand the chronological character for formation of first C–C bonds in order to demonstrate the competition between HETD and HOMD cycloadditions (Figure 7).[56-62] 44 and 63 trajectories were generated starting from the TSs **8⁺** and **11⁺**, respectively, in which forward and backward propagations (t = 0 fs) are initiated showing the typical reactive bonds toward either cationic uncyclized intermediates (**9⁺** and **12⁺**) or reactants (styrene **4⁺**, **4** and **5**). No recrossing is observed in our simulation. The C3–C4 distance is rapidly shortened to ~1.6 Å in most trajectories, and the bond remains in the whole trajectory once formed although for

a small proportion of trajectories the C3–C4 distance oscillates in the range between 1.6 Å and 2.0 Å. By recording the timing for the C3–C4 distance to be shortened below 1.6 Å, we obtained the average timing for the first C–C bond formation at 43.0 and 47.0 fs for HETD 8^+ and HOMD 11^+, respectively. It is interesting that although the average timing is similar, there are more trajectories exhibiting larger timing for C–C bond formation for the HOMD pathway, which may indicate a flatter potential energy surface in the post-transition state period. Comparison of the average time for the first C–C bond formation through TS 8^+ and TS 11^+ reveals a short timing gap of 4.0 fs. Also, the timing for first C–C bond formation for the unstacked TSs were obtained and shown a short timing gap where 46 fs for HOMD, derived from 24 trajectories, and 44 fs for HETD, derived from 20 trajectories (see Figure S3 in ESI). Overall, the very small timing gap between both pathways is in good consistence with the coexistence of HETD and HOMD pathways and explain why both pathways are competitive.
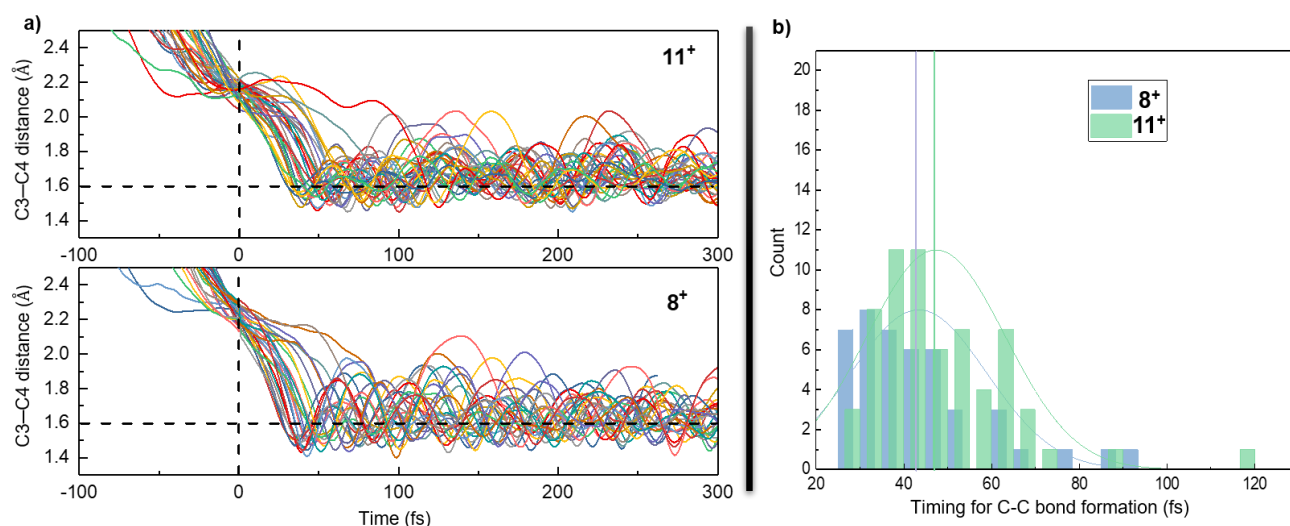
Figure 7. (a) Evolution of the C–C distance corresponding to the first C–C bond formation along quasiclassical trajectories initialized from TSs 8^+ and 11^+ calculated by the wB97XD/6-31G(d) level of theory. All trajectories start from the initial geometry (t = 0 fs) generated by adding a random displacement to the transition state, and both directions are shown in positive and negative part of the horizontal axis. (b) A histogram for the C–C bond formation timing, where the average timing for each reaction is shown by the vertical line.

Stability of the SEO step

The stability of the radical cations and anions formed from the SEO step can be rationalized at least qualitatively on the basis of frontier molecular orbital analysis. Simply, removing an electron from styrene **4**, represented as highest occupied molecular orbitals (HOMO), to the HVIR, represented as lowest unoccupied molecular orbitals (LUMO), generates the radical anion and cation. These charged species are generally stabilized by the frontier orbitals of the charged radicals, where HOMOs for anions and LUMOs for cation.

FMO of radical cation 4⁺. The HOMOs on styrene **4** are a combination of two degenerate HOMOs (HOMO and HOMO–1) came from the double bond and *para*-phenyl ring (Figure 8-a). The SEO leads to stabilizations for cations to be achieved from HOMOs and LUMOs. As shown in Figure 8-a, removal of an electron from HOMO of styrene **4** splits its HOMO into β-LUMO and α-SOMO (singly occupied MO). The removal of electron from the HOMO lessens the HOMO energy to more than half because the orbital is singly- rather than doubly-occupied. Secondly, a stabilization in the LUMO of radical cation **4⁺** raises to more than double after electron removal. Thirdly, the remaining two electrons in the HOMO–1 have bonding interactions and a preference for radical cation to adopt interaction is existed. At this point, the radical cation gains stabilizations when the HOMO is no longer doubly occupied because the unpaired electron is delocalized by which a prominent π electron delocalization distributed from the styrene double bond to the phenyl ring. The spin density, $\rho_{(\alpha)} - \rho_{(\beta)}$, provides information about the localization of the unpaired electron. While the calculated spin density is majorly accounted from the HOMOs (HOMO energy is $\alpha = -12.15$ eV and $\beta = -6.79$ eV), the contours of the spin density clearly display an entire delocalization over the system (see blue box in Figure 8-a) although the contour for spin density is similar to the SOMO.

Under HFIP SEO conditions, the oxidants **DMP$_{HFIP}$** and **PIDA$_{HFIP}$** acquire stabilizations before and after electron addition, majorly attributed to the hydrogen bonding interactions that substantially lower the energy of the LUMOs and at some level the HOMOs. Therefore, we will discuss these stabilities as before and after electron addition.

FMO of radical anions DMP⁻$_{HFIP}$ and PIDA⁻$_{HFIP}$. The effect of electron addition on splitting of LUMOs for HVIRs with and without hydrogen bonding is shown in Figure 8-b,c. Further visualizations of FMOs for **DMP⁻** and **PIDA⁻** are provided in ESI. In the case of **DMP$_{HFIP}$**, the electron is added to the LUMO leading to split its orbitals into α-SOMO and β-LUMO. This lessens the raise in α-SOMO energy to more than triple times of the LUMO but it decreases the stability of β-LUMO (Figure 8-b). In the case of **PIDA$_{HFIP}$**, addition of an electron makes the energy of SOMO stabilized by more than seven times of the LUMO with the β-LUMO being slightly stabilized too (Figure 8-c). The unpaired electron is localized on the iodine center, perpendicularly to the phenyl ring as indicated by the orbital contours of SOMO and spin density for **DMP⁻$_{HFIP}$** and **PIDA⁻$_{HFIP}$**. Noticeably, we have seen that initiation by **DMP$_{HFIP}$** is more thermodynamically favorable than by **PIDA$_{HFIP}$**. A reasonable explanation would be more likely emerged from the fact that the SOMO energy of the **DMP⁻$_{HFIP}$** is lower than the **PIDA⁻$_{HFIP}$** in addition to the energy gaps of electron transfer in a SEO step by I(V) **DMP$_{HFIP}$** is lower than I(III) **PIDA$_{HFIP}$** (Figure 8-b,c and Table 1).
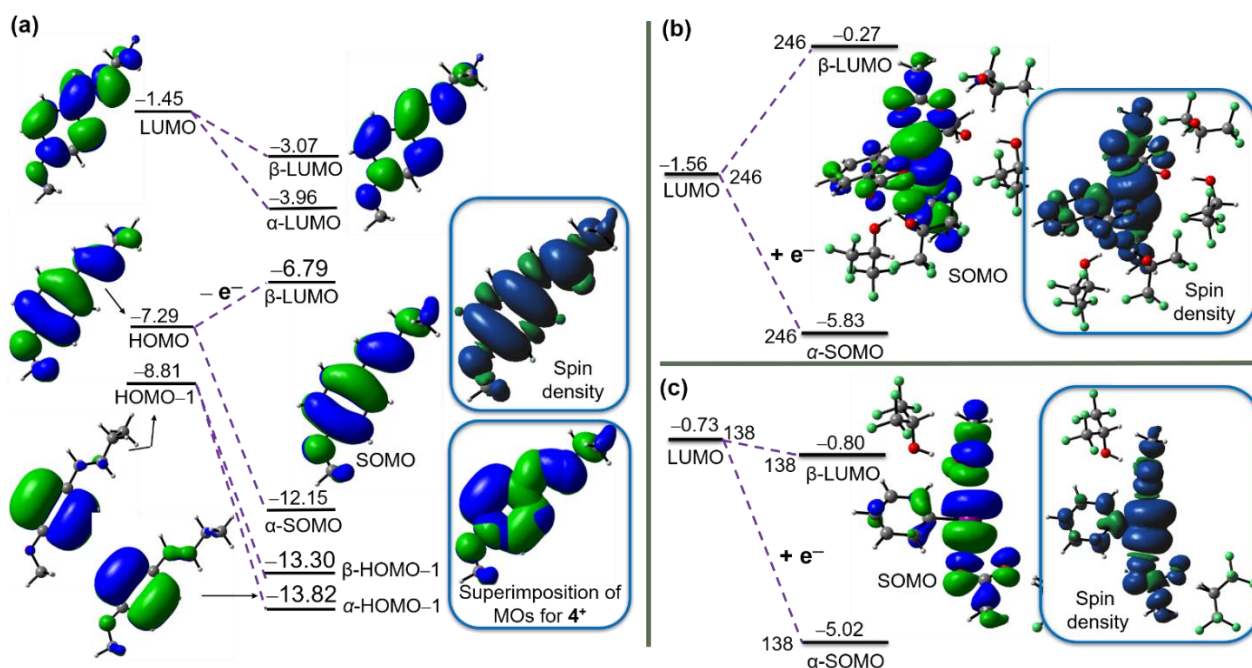
Figure 8. (a) Involvement of the FMOs for **4** before (left) and after (right) electron removal. The removal of an electron splits the HOMO into β-LUMO and α-SOMO that have identical wave functions. (b) Splitting of LUMO into α-SOMO and β-LUMO after electron addition to **DMP**$_{\text{HFIP}}$ (a) and **PIDA**$_{\text{HFIP}}$ (b). Spin density of the correspondent radical cations and anions are in blue box.

FMO of neutral DMP$_{\text{HFIP}}$ **and PIDA**$_{\text{HFIP}}$. The effect of hydrogen bonding interactions on stability of the HOMOs and LUMOs accounted for neutral HVIRs before electron addition is presented in Figure 9. Two important information can be seen from Figure 9. First, the hydrogen bonding generally lessens the energy of LUMOs and HOMOs of **DMP** and **PIDA**. The impact of lowering the energetic levels of LUMOs is seen to be greater on **DMP**$_{\text{HFIP}}$ than **PIDA**$_{\text{HFIP}}$. The LUMO energy of **DMP**$_{\text{HFIP}}$ decreases by around 1.04 eV (–0.52 → –1.56 eV, Figure 9-a) whereas a lower decrease of 0.82 eV (+0.09 → –73 eV, Figure 9-b) is obtained for **PIDA**$_{\text{HFIP}}$. LUMO+1, which is in the plane of phenyl ring, and LUMO+2, which is the antibonding orbitals for the phenyl ring, are stabilized by 1.01 eV (–0.27 → –1.28 eV) and 0.81 eV (+0.36 → –0.45 eV) for **DMP**, respectively. For **PIDA**, LUMO+1 and LUMO+2 are stabilized by 0.63 eV (+0.68 → +0.05 eV) and 0.38 (+1.28 → +0.90 eV), respectively. This indicates that hydrogen bonding makes the iodine more deficient by lowering the energy of antibonding orbitals.

Second, stabilization of the HOMOs is also seen but the effect on **DMP** is different. The HOMO orbitals on **PIDA** have similar contours before and after **PIDA** being hydrogen bonded. The HOMO and HOMO-1 that were belong to the axial and equatorial (to the plane of phenyl ring) antibonding orbitals on **DMP** become located on HFIP molecules, specifically on the OH of HFIP, although HFIP is low nucleophilic solvent. This would indicate that the effect of nucleophilicity of acetate groups on iodine decreases substantially when they are hydrogen bonded. This case is not seen in I(III) **PIDA** because **DMP** is already higher oxidation state in which hydrogen bonding makes I(V) more deficient and reactive reagent. Overall, HIFP lowers the HOMOs of

acetate groups and, subsequently, the LUMO of the iodine center decreases to a level that makes it a capable species for SEO.
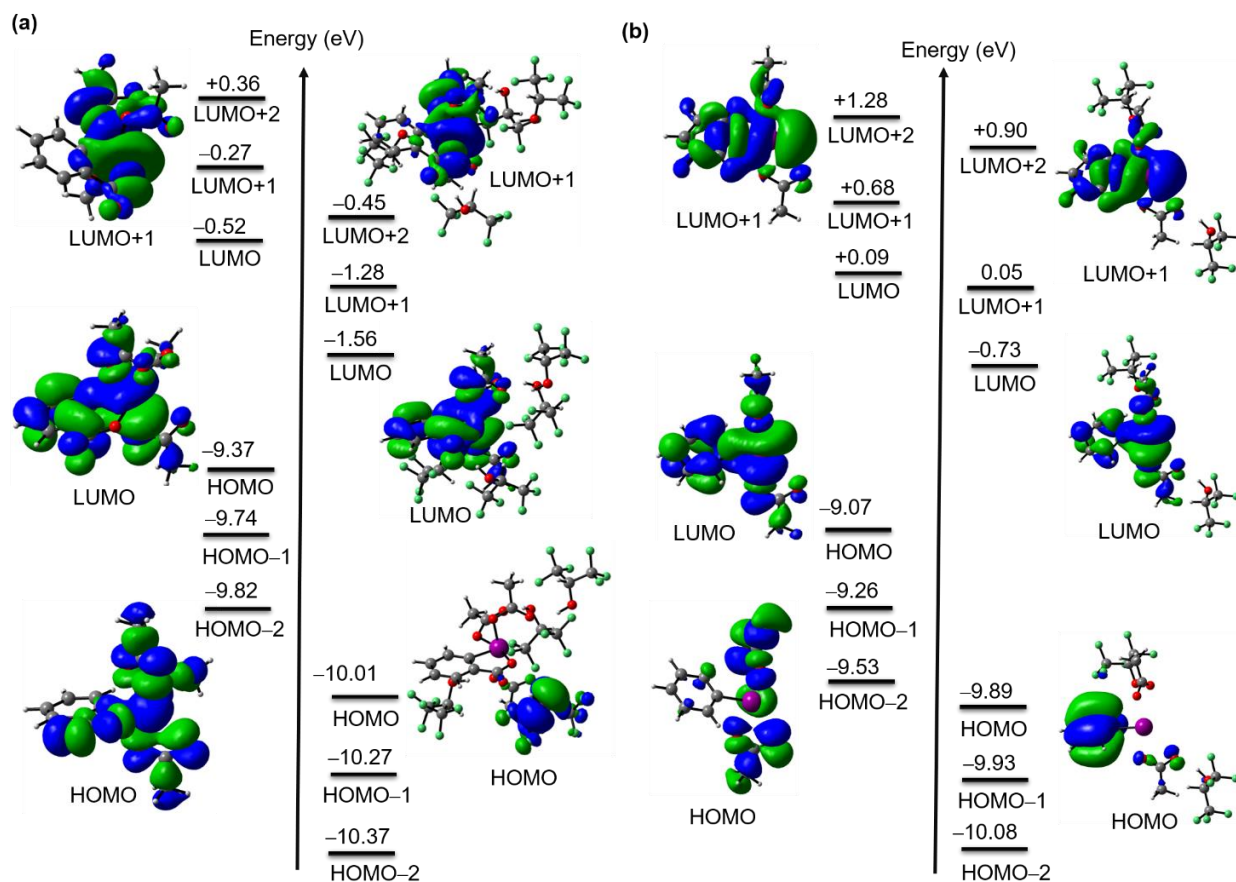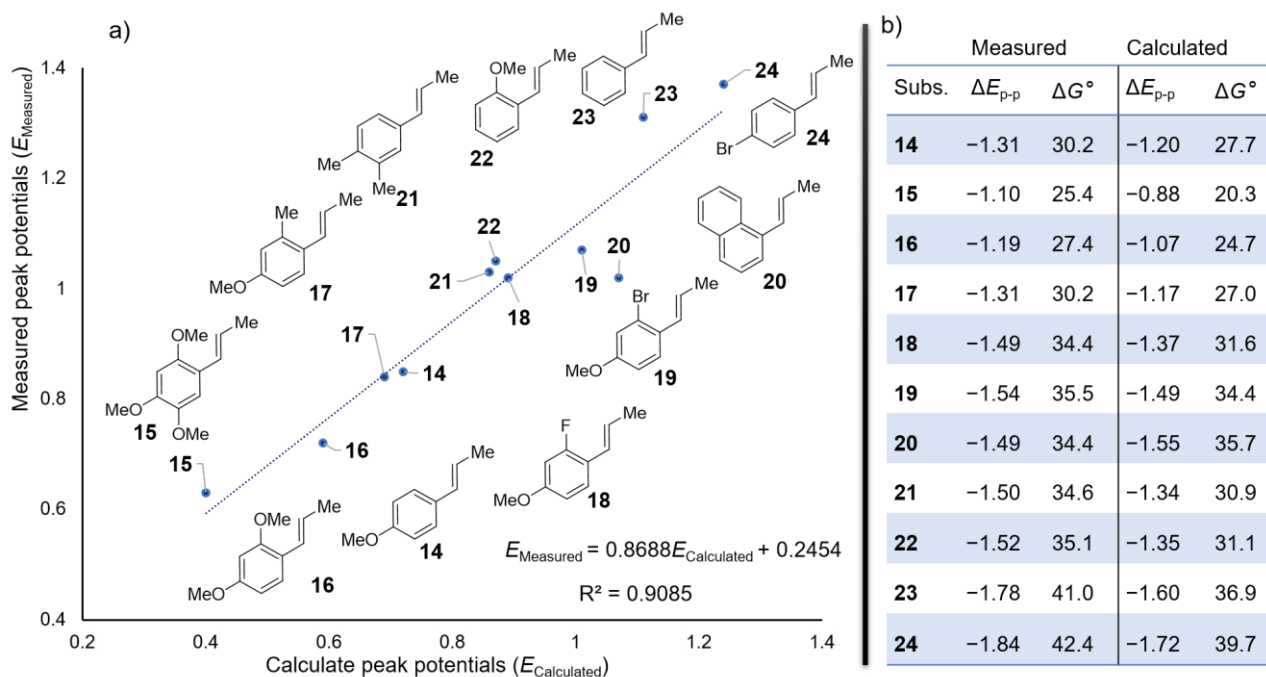

Figure 9. FMOs of the **DMP** (a) and **PIDA** (b) before electron addition, showing the effect of hydrogen bonding interactions on stabilities of the HOMOs and LUMOs of each reagent. The contours of the other orbitals are shown in SI.

Effect of substituents on SEO

Based on the above findings, we have investigated the effect of substituents on the SEO to gain a broader vision that makes a styrene successfully active. First, comparison between calculated and measured redox potentials of different substituted *trans-β*-methylstyrenes **14 − 24** is indicated in Figure 10. Our strategic DFT simulations present a very good agreement with the experimental redox potentials and free energy of reoxidation accordingly. The explicit-involved HFIP calculations are consistent with experimental results than inexplicit calculations (for comparison see ESI). The calculated results appeared in Figure 10-b indicate is a deviation from experimental values of around 0.12 eV which is in agreement with the mean absolute error in ionization energy (2.74 kcal mol^{-1}) reported for *w*B97XD.[63] Notably, the measured and calculated potentials refer to the important role of a *p*-methoxy group in the success of a styrene toward dimerization, however, the absence of *p*-methoxy motif resulted in unsuccessful dimerization with **PIDA**/HFIP.[43] Using voltammetric oxidation peak potentials to understand the reactivity is relatively evident. Styrenes with high voltammetric oxidation potentials

failed to undergo [2+2] cycloaddition under **PIDA**/HFIP conditions due to the initiation (SEO, FRS) become comparatively thermodynamically disfavorable, especially for more electron deficient styrenes. Styrenes **14 – 19** were synthetically reactive and **20 − 24** were unreactive.[43] Broadly saying, and as indicated by Donohoe and co-workers it seems that the styrenes that exhibit oxidative peak potentials ($E_{p,a}$) below ∼ +1.0 V vs Fc/Fc⁺ in HFIP lead to [2+2] cycloaddition product although the correlation seems relatively not applied on the productive styrenes **18** and **19** and the unproductive styrenes **20** and **21** when subject to **PIDA**/HFIP conditions. Further DFT investigations on the initiation step by **PIDA$_{HFIP}$** of these styrenes are shown in Table 1. The results are compared with those predicted by **DMP$_{HFIP}$** (Table 1). Experimentally, the styrenes **14 – 24** were tested only with **PIDA$_{HFIP}$** and, for the first instance, we thought that it is reasonable to theoretically evaluate their reactivities toward higher oxidation state of HVIR. We will first explain the results of SEO by **PIDA$_{HFIP}$**.

	Measured		Calculated	
Subs.	$\Delta E_{p\text{-}p}$	$\Delta G°$	$\Delta E_{p\text{-}p}$	$\Delta G°$
14	−1.31	30.2	−1.20	27.7
15	−1.10	25.4	−0.88	20.3
16	−1.19	27.4	−1.07	24.7
17	−1.31	30.2	−1.17	27.0
18	−1.49	34.4	−1.37	31.6
19	−1.54	35.5	−1.49	34.4
20	−1.49	34.4	−1.55	35.7
21	−1.50	34.6	−1.34	30.9
22	−1.52	35.1	−1.35	31.1
23	−1.78	41.0	−1.60	36.9
24	−1.84	42.4	−1.72	39.7

$E_{Measured} = 0.8688 E_{Calculated} + 0.2454$

$R^2 = 0.9085$

Figure 10. (a) Agreement between measured and calculated voltammetric peak potentials (in V) for redox species of different substituted *trans-β*-methylstyrenes **14 – 24**. (b) Differences in the reduction and oxidation peak potentials (in V) and their Gibbs free energies (in kcal mol⁻¹) for styrenes **14 – 24**. Styrenes **20 – 24** did not undergo **PIDA** [2+2] cycloaddition. The measured results were obtained versus Fc/Fc⁺, as measured at 100 mV s⁻¹ taken from ref 43. The calculated Fc/Fc⁺ is $E^{1/2} = 4.84$ V in HFIP. The calculated value for **PIDA$_{HFIP}$** + e⁻ → **PIDA⁻$_{HFIP}$** is $E^{1/2} = 4.25$ V. Measured peak potential for **PIDA** is $E_{p,c} = −0.47$ V. [43] Th calculated peak potential for **PIDA$_{HFIP}$** $E_{p,c} = −0.59$ V.

The DFT calculations on MOs analysis clearly evidence that from the top to the down of the table the more electron-rich styrene system the highest HOMOs and the more reactive toward the SEO, i. e. HOMOs decrease from the top to the down of the table. Following an electron removal from styrenes, the stability of the degenerated orbitals, α-SOMO and β-LUMO, increase with the decrease in the HOMOs. In this regard, the calculated energy gaps for an electron transfer to **PIDA$_{HFIP}$** (E_g^c = LUMO[**PIDA$_{HFIP}$**] − HOMO[styrene])

increase from the top to the down of the table with the highest one reported for the styrene **24** (Table 1). The energy barriers of initiation for substrates **14 – 24** indicated in Table 1 have a correlation with experimental $E_{p,a}$ peak potentials and Gibbs free energy of SEO step. Those substrates with low experimental $E_{p,a}$ have low ΔG_r and correspondingly lower $\Delta G^{\ddagger}$ and vice versa. The SEO step that leads to a more thermodynamically favorable radical cation formation makes the cycloaddition more successful, but this is more likely dependent on the kinetics of this step that requires Gibbs free energy (ΔG_r) and reorganization energy (λ) based on Marcus theory. However, it turns out that the calculated barriers for all styrenes indicate that the thermodynamic term represents a major contribution in the initiative barrier, and the reorganization term evidently becomes less effective. In agreement with the experimental findings, the unreactive styrenes **20 – 24** were found to undergo highly initiative barriers whereas reactive styrenes **14 – 19** are generally require lower energy to initiate the reaction. Furthermore, a good correlation between the calculated FMO energies and free energies of activation and reaction is relatively apparent. The removal of an electron from a low HOMO styrene gives a low α-SOMO and β-LUMO radical cation and this, consequently, leads to a lower energy gap and free energy of activation.

Table 1. Calculated energies for the SEO step by I(III) **PIDA**$_{\text{HFIP}}$ and **DMP**$_{\text{HFIP}}$ of different substituted *trans-β*-methylstyrenes **14 – 24**.[a]

| | FMO energies (eV)[b] | | | | | Energy of SEO (kcal mol^{-1}) | | | |
| | | | | | | **PIDA**$_{\text{HFIP}}$ | | **DMP**$_{\text{HFIP}}$ | |
Styren	HOMO	α-	β-LUMO	$E_g{}^c$	$E_g{}^d$	ΔG_r	$\Delta G^{\ddagger}$	ΔG_r	$\Delta G^{\ddagger}$
14	−7.27	−12.22	−6.83	6.54	5.71	28.6	31.6	13.5	19.9
15	−7.18	−11.33	−6.06	6.45	5.62	20.3	30.7	6.6	21.2
16	−7.04	−11.87	−6.45	6.31	5.48	24.8	28.8	10.5	18.0
17	−7.28	−12.11	−6.73	6.55	5.72	27.1	30.5	12.7	19.5
18	−7.41	−12.34	−6.95	6.68	5.85	34.5	35.4	20.1	23.1
19	−7.69	−12.33	−7.01	6.96	6.13	31.6	34.0	17.3	22.4
20	−7.44	−12.03	−6.96	6.71	5.88	54.0	37.5	21.5	25.5
21	−7.53	−12.63	−7.11	6.80	5.97	31.1	33.4	16.8	21.8
22	−7.39	−12.53	−7.00	6.66	5.83	31.4	33.6	17.1	22.0
23	−7.79	−13.21	−7.54	7.06	6.23	36.9	38.1	22.6	25.8
24	−7.96	−12.82	−7.59	7.23	6.40	39.7	40.1	25.4	27.1

[a] The calculations were carried out with hydrogen-bonded iodine reagents. [b] Calculations were performed in gas phase with *w*B97XD/6-31G(d)/LANL2DZ level of theory, and the LUMO of **DMP**$_{\text{HFIP}}$ is −1.56 eV and the LUMO of **PIDA**$_{\text{HFIP}}$ is −0.73 eV. Removal an electron from styrene splits the HOMO into α-SOMO and β-LUMO. [c] Energy gap (E_g) = LUMO[**PIDA**$_{\text{HFIP}}$] – HOMO[styrene]. [d] Energy gap (E_g) = LUMO[**DMP**$_{\text{HFIP}}$] – HOMO[styrene].

Next, we explored the reactivity of these styrenes toward the SEO by DMP_{HFIP} although experimentally not reported (Table 1). Expectedly, as we have seen above that iodine (V) is more reactive toward SEO, DMP_{HFIP} gave a lower initiative energy than by $PIDA_{HFIP}$ although the same trend toward reactivity has been obtained. The substrates that are not synthetically active are also shown higher initiative SEO by DMP_{HFIP} except **21** and **22**. The free energy of activation for SEO by DMP_{HFIP} is significantly lower than for that obtained with $PIDA_{HFIP}$ even for those who are not reactive toward cycloaddition. The energy gaps ($E_g^c = LUMO[DMP_{HFIP}]$ – HOMO[styrene]) calculated with DMP_{HFIP} is lower than from those calculated for $PIDA_{HFIP}$ by 0.83 eV. These results reveal that DMP_{HFIP} is more reactive toward SEO than $PIDA_{HFIP}$. Overall, the calculated energies gave a good insight into reactivity of these styrenes toward cycloaddition and will raise a new understanding toward further attentions to advance further investigations.

Conclusions

DFT calculations at the (SMD)-wB97XD/Def2-TZVPP,6-311+G(d,p)//wB97XD/6-31G(d),LANL2DZ level of theory were exploited to provide mechanistic insights into the HVIR-promoted hetero- and homodimerizations of styrenes facilitated by HFIP. The computational level was validated through comparison between calculated and measured redox potentials of different substituted *trans-β*-methylstyrenes. The findings achieved in this study can be summarized as follows.

1- The HFIP molecules lower the energy of the single electron oxidation (SEO) or initiation as a result of strong hydrogen bonding interactions that substantially lower the energy of the frontier orbitals before and after electron addition.

2- The mechanism of HETD and HOMD is a radically-characterized π-π stacked head-to-head stepwise [2+2] cycloaddition initiated via SEO by **DMP** and **PIDA**, respectively. DFT results supported by quasiclassical molecular dynamics simulations show that HOMD is a competing pathway to HETD although the latter is relatively faster, in accordance with experimental observations.

3- The initiation is a rate-determining step as a thermodynamically endergonic and propagation is accomplished by radically-cationic hetero- and homodimerized intermediates and propagation is faster than termination by radically-anionic HVIRs.

4- Initiation by DMP_{HFIP} found to be faster and thermodynamically more favorable than by $PIDA_{HFIP}$ due to (1) the SOMO energy of the radical anion DMP^-_{HFIP} is lower than $PIDA^-_{HFIP}$ and (2) the calculated energy gap of electron transfer for a SEO ($E_g = LUMO[HVIR]$ – HOMO[styrene]) by DMP_{HFIP} is lower than $PIDA_{HFIP}$ by 0.83 eV.

5- Comparison between the measured and calculated redox potentials evaluated the important role of a *p*-methoxy group in the success of a styrene toward dimerization. We found that the SEO step that leads to a more thermodynamically favorable radical cation formation makes the cycloaddition more successful, indicating that the thermodynamic term represents a major contribution in the initiative barrier.

Overall, this mechanistic study brings significantly important insights into a such influential synthetic utility and opens possibilities toward advancing an efficient protocol for stereoselective approaches of simple and complex hetero- and homodimerizations. We envision that using DFT simulations on catalyzed SEO will enhance and warrant further attentions toward developing various oxidants to synthetically access a wide range of substrates used for bioactive and synthetic cyclobutane-containing products in a more efficiently-controlled fashion.

Conflicts of interest

There are no conflicts to declare.

Acknowledgements

References

1.   Xu, Y.; Conner, M. L.; Brown, M. K., Cyclobutane and Cyclobutene Synthesis: Catalytic Enantioselective 2+2 Cycloadditions. *Angewandte Chemie-International Edition* **2015,** *54* (41), 11918-11928.

2.   Margaretha, P., Retrospective View on Recent Developments in Cyclobutane Synthesis via [2+2] Photocycloaddition of Unsaturated Ketones to Acyclic Dienes. *Helvetica Chimica Acta* **2014,** *97* (7), 1027-1035.

3.   Dembitsky, V. M., Naturally occurring bioactive Cyclobutane-containing (CBC) alkaloids in fungi, fungal endophytes, and plants. *Phytomedicine* **2014,** *21* (12), 1559-1581.

4.   Dembitsky, V. M., Bioactive cyclobutane-containing alkaloids. *Journal of Natural Medicines* **2008,** *62* (1), 1-33.

5.   Cretton, S.; Bartholomeusz, T. A.; Jeannerat, D.; Munoz, O.; Christen, P.; Hostettmann, K., New cyclobutane-containing tropane alkaloids from the aerial parts of Schizanthus grahamii. *Planta Medica* **2009,** *75* (9), 916-916.

6.   Ito, H.; Toyoda, T.; Sawamura, M., Stereospecific Synthesis of Cyclobutylboronates through Copper(I)-Catalyzed Reaction of Homoallylic Sulfonates and a Diboron Derivative. *Journal of the American Chemical Society* **2010,** *132* (17), 5990-5992.

7.   Noucti, N. N.; Alexanian, E. J., Stereoselective Nickel- Catalyzed 2+2 Cycloadditions of EneAllenes. *Angewandte Chemie-International Edition* **2015,** *54* (18), 5447-5450.

8.   Gulías, M.; Collado, A.; Trillo, B.; López, F.; Oñate, E.; Esteruelas, M. A.; Mascareñas, J. L., Ruthenium-Catalyzed (2 + 2) Intramolecular Cycloaddition of Allenenes. *Journal of the American Chemical Society* **2011,** *133* (20), 7660-7663.

9.   Luzung, M. R.; Mauleón, P.; Toste, F. D., Gold(I)-Catalyzed [2 + 2]-Cycloaddition of Allenenes. *Journal of the American Chemical Society* **2007,** *129* (41), 12402-12403.

10.   Chiba, K.; Miura, T.; Kim, S.; Kitano, Y.; Tada, M., Electrocatalytic Intermolecular Olefin Cross-Coupling by Anodically Induced Formal [2+2] Cycloaddition between Enol Ethers and Alkenes. *Journal of the American Chemical Society* **2001,** *123* (45), 11314-11315.

11.   Rath, B. B.; Kole, G. K.; Morris, S. A.; Vittal, J. J., Rotation of a helical coordination polymer by mechanical grinding. *Chemical Communications* **2020**.

12.   Ledwith, A., Cation radicals in electron transfer reactions. *Accounts of Chemical Research* **1972,** *5* (4), 133-139.

13.   Bell, F. A.; Crellin, R. A.; Fujii, H.; Ledwith, A., Cation-radicals: metal-catalysed cyclodimerisation of aromatic enamines. *Journal of the Chemical Society D: Chemical Communications* **1969,** (6), 251-252.

14.   Bauld, N. L.; Bellville, D. J.; Harirchian, B.; Lorenz, K. T.; Pabon, R. A.; Reynolds, D. W.; Wirth, D. D.; Chiou, H. S.; Marsh, B. K., Cation radical pericyclic reactions. *Accounts of Chemical Research* **1987,** *20* (10), 371-378.

15.   Bauld, N. L.; Bellville, D. J.; Pabon, R.; Chelsky, R.; Green, G., Theory of cation-radical pericyclic reactions. *Journal of the American Chemical Society* **1983,** *105* (8), 2378-2382.

16.   Bauld, N. L.; Pabon, R., Cation radical catalyzed olefin cyclodimerization. *Journal of the American Chemical Society* **1983,** *105* (3), 633-634.

17.   Ischay, M. A.; Ament, M. S.; Yoon, T. P., Crossed intermolecular [2 + 2] cycloaddition of styrenes by visible light photocatalysis. *Chemical Science* **2012,** *3* (9), 2807-2811.

18.   Riener, M.; Nicewicz, D. A., Synthesis of cyclobutane lignans via an organic single electron oxidant–electron relay system. *Chemical Science* **2013,** *4* (6), 2625-2629.

19.   Jiang, Y.; Wang, C.; Rogers, C. R.; Kodaimati, M. S.; Weiss, E. A., Regio- and diastereoselective intermolecular [2+2] cycloadditions photocatalysed by quantum dots. *Nature Chemistry* **2019,** *11* (11), 1034-1040.

20.   Ischay, M. A.; Lu, Z.; Yoon, T. P., [2+2] Cycloadditions by Oxidative Visible Light Photocatalysis. *Journal of the American Chemical Society* **2010,** *132* (25), 8572-8574.

21.   Lu, Z.; Yoon, T. P., Visible Light Photocatalysis of [2+2] Styrene Cycloadditions by Energy Transfer. *Angewandte Chemie International Edition* **2012,** *51* (41), 10329-10332.

22.   Hurtley, A. E.; Lu, Z.; Yoon, T. P., [2+2] Cycloaddition of 1,3-Dienes by Visible Light Photocatalysis. *Angewandte Chemie International Edition* **2014,** *53* (34), 8991-8994.

23.   Fleming, S. A.; Ward, S. C., Stereocontrolled photochemical [2 + 2] cycloaddition. *Tetrahedron Letters* **1992,** *33* (8), 1013-1016.

24.   Ward, S. C.; Fleming, S. A., [2 + 2] Photocycloaddition of Cinnamyloxy Silanes. *The Journal of Organic Chemistry* **1994,** *59* (21), 6476-6479.

25.   Horibe, T.; Katagiri, K.; Ishihara, K., Radical-Cation-Induced Crossed [2+2] Cycloaddition of Electron-Deficient Anetholes Initiated by Iron(III) Salt. *Advanced Synthesis & Catalysis* **2020,** *362* (4), 960-963.

26.   Zhao, L.-M.; Lei, T.; Liao, R.-Z.; Xiao, H.; Chen, B.; Ramamurthy, V.; Tung, C.-H.; Wu, L.-Z., Visible-Light-Triggered Selective Intermolecular [2+2] Cycloaddition of Extended Enones: 2-Oxo-3-enoates and 2,4-Dien-1-ones with Olefins. *The Journal of Organic Chemistry* **2019,** *84* (14), 9257-9269.

27.   Li, R.; Ma, B. C.; Huang, W.; Wang, L.; Wang, D.; Lu, H.; Landfester, K.; Zhang, K. A. I., Photocatalytic Regioselective and Stereoselective [2 + 2] Cycloaddition of Styrene Derivatives Using a Heterogeneous Organic Photocatalyst. *ACS Catalysis* **2017,** *7* (5), 3097-3101.

28.   Amjaour, H.; Wang, Z.; Mabin, M.; Puttkammer, J.; Busch, S.; Chu, Q. R., Scalable preparation and property investigation of a cis-cyclobutane-1,2-dicarboxylic acid from β-trans-cinnamic acid. *Chemical Communications* **2019,** *55* (2), 214-217.

29.   Yoshimura, A.; Zhdankin, V. V., Advances in Synthetic Applications of Hypervalent Iodine Compounds. *Chemical Reviews* **2016,** *116* (5), 3328-3435.

30.   Li, Y.; Hari, D. P.; Vita, M. V.; Waser, J., Cyclic Hypervalent Iodine Reagents for Atom-Transfer Reactions: Beyond Trifluoromethylation. *Angewandte Chemie International Edition* **2016,** *55* (14), 4436-4454.

31.   Colomer, I.; Chamberlain, A. E. R.; Haughey, M. B.; Donohoe, T. J., Hexafluoroisopropanol as a highly versatile solvent. *Nature Reviews Chemistry* **2017,** *1* (11), 0088.

32.   Zhu, Y.; Colomer, I.; Thompson, A. L.; Donohoe, T. J., HFIP Solvent Enables Alcohols To Act as Alkylating Agents in Stereoselective Heterocyclization. *Journal of the American Chemical Society* **2019,** *141* (16), 6489-6493.

33.   Colomer, I.; Barcelos, R. C.; Christensen, K. E.; Donohoe, T. J., Orthogonally Protected 1,2-Diols from Electron-Rich Alkenes Using Metal-Free Olefin syn-Dihydroxylation. *Organic Letters* **2016,** *18* (22), 5880-5883.

34.   Raheem, I. T.; Thiara, P. S.; Peterson, E. A.; Jacobsen, E. N., Enantioselective Pictet−Spengler-Type Cyclizations of Hydroxylactams: H-Bond Donor Catalysis by Anion Binding. *Journal of the American Chemical Society* **2007,** *129* (44), 13404-13405.

35. Lv, H.; Zhan, J.-H.; Cai, Y.-B.; Yu, Y.; Wang, B.; Zhang, J.-L., π–π Interaction Assisted Hydrodefluorination of Perfluoroarenes by Gold Hydride: A Case of Synergistic Effect on C–F Bond Activation. *Journal of the American Chemical Society* **2012,** *134* (39), 16216-16227.

36. Doyle, A. G.; Jacobsen, E. N., Small-Molecule H-Bond Donors in Asymmetric Catalysis. *Chemical Reviews* **2007,** *107* (12), 5713-5743.

37. Nicolaou, K. C.; Baran, P. S.; Zhong, Y.-L.; Vega, J. A., Novel IBX-Mediated Processes for the Synthesis of Amino Sugars and Libraries Thereof. *Angewandte Chemie International Edition* **2000,** *39* (14), 2525-2529.

38. Nicolaou, K. C.; Baran, P. S.; Zhong, Y. L.; Barluenga, S.; Hunt, K. W.; Kranich, R.; Vega, J. A., Iodine(V) Reagents in Organic Synthesis. Part 3. New Routes to Heterocyclic Compounds via o-Iodoxybenzoic Acid-Mediated Cyclizations: Generality, Scope, and Mechanism. *Journal of the American Chemical Society* **2002,** *124* (10), 2233-2244.

39. Nicolaou, K. C.; Baran, P. S.; Kranich, R.; Zhong, Y.-L.; Sugita, K.; Zou, N., Mechanistic Studies of Periodinane-Mediated Reactions of Anilides and Related Systems. *Angewandte Chemie International Edition* **2001,** *40* (1), 202-206.

40. Janza, B.; Studer, A., Stereoselective Cyclization Reactions of IBX-Generated Alkoxyamidyl Radicals. *The Journal of Organic Chemistry* **2005,** *70* (17), 6991-6994.

41. Colomer, I.; Coura Barcelos, R.; Donohoe, T. J., Catalytic Hypervalent Iodine Promoters Lead to Styrene Dimerization and the Formation of Tri- and Tetrasubstituted Cyclobutanes. *Angewandte Chemie International Edition* **2016,** *55* (15), 4748-4752.

42. Zhu, Y.; Colomer, I.; Donohoe, T. J., Hypervalent iodine initiated intramolecular alkene dimerisation: a stereodivergent entry to cyclobutanes. *Chemical Communications* **2019,** *55* (69), 10316-10319.

43. Colomer, I.; Batchelor-McAuley, C.; Odell, B.; Donohoe, T. J.; Compton, R. G., Hydrogen Bonding to Hexafluoroisopropanol Controls the Oxidative Strength of Hypervalent Iodine Reagents. *Journal of the American Chemical Society* **2016,** *138* (28), 8855-8861.

44. Farshadfar, K.; Chipman, A.; Yates, B. F.; Ariafard, A., DFT Mechanistic Investigation into BF3-Catalyzed Alcohol Oxidation by a Hypervalent Iodine(III) Compound. *ACS Catalysis* **2019,** *9* (7), 6510-6521.

45. Ganji, B.; Ariafard, A., DFT mechanistic investigation into phenol dearomatization mediated by an iodine(iii) reagent. *Organic & Biomolecular Chemistry* **2019,** *17* (14), 3521-3528.

46. Kaur, A.; Ariafard, A., Mechanistic investigation into phenol oxidation by IBX elucidated by DFT calculations. *Organic & Biomolecular Chemistry* **2020,** *18* (6), 1117-1129.

47. De Munari, S.; Frigerio, M.; Santagostino, M., Hypervalent Iodine Oxidants: Structure and Kinetics of the Reactive Intermediates in the Oxidation of Alcohols and 1,2-Diols by o-Iodoxybenzoic Acid (IBX) and Dess−Martin Periodinane. A Comparative 1H-NMR Study. *The Journal of Organic Chemistry* **1996,** *61* (26), 9272-9279.

48. O'Nei, L. L.; Wiest, O., Acyclic or Long-Bond Intermediate in the Electron-Transfer-Catalyzed Dimerization of 4-Methoxystyrene. *The Journal of Organic Chemistry* **2006,** *71* (23), 8926-8933.

49.	Guo, C.; Cui, L.; Chen, B.; Yuan, J.; Tian, Z., A theoretical study on the stereoconvergency of the intramolecular radical cation [2+2] cycloadditions of bis(styrenes). *RSC Advances* **2012,** *2* (26), 9932-9937.

50.	Li, Y.; Guo, C.; Chen, B.-Z., A theoretical study on intermolecular [2+2] radical cation cycloaddition reactions and the competition between concerted and stepwise mechanisms. *Computational and Theoretical Chemistry* **2016,** *1078*, 163-172.

51.	Nelsen, S. F.; Blackstock, S. C.; Kim, Y., Estimation of inner shell Marcus terms for amino nitrogen compounds by molecular orbital calculations. *Journal of the American Chemical Society* **1987,** *109* (3), 677-682.

52.	Vaissier, V.; Barnes, P.; Kirkpatrick, J.; Nelson, J., Influence of polar medium on the reorganization energy of charge transfer between dyes in a dye sensitized film. *Physical Chemistry Chemical Physics* **2013,** *15* (13), 4804-4814.

53.	Manke, F.; Frost, J. M.; Vaissier, V.; Nelson, J.; Barnes, P. R. F., Influence of a nearby substrate on the reorganization energy of hole exchange between dye molecules. *Physical Chemistry Chemical Physics* **2015,** *17* (11), 7345-7354.

54.	Demaille, C.; Bard, A. J., Kinetics and mechanism of the anodic dimerization of trans-anethole studied by cyclic voltammetry and scanning electrochemical microscopy. *Acta Chemica Scandinavica* **1999,** *53* (10), 842-848.

55.	Johnson, E. R.; Keinan, S.; Mori-Sánchez, P.; Contreras-García, J.; Cohen, A. J.; Yang, W., Revealing Noncovalent Interactions. *Journal of the American Chemical Society* **2010,** *132* (18), 6498-6506.

56.	Burns, J. M.; Boittier, E. D., Pathway Bifurcation in the (4 + 3)/(5 + 2)-Cycloaddition of Butadiene and Oxidopyrylium Ylides: The Significance of Molecular Orbital Isosymmetry. *The Journal of Organic Chemistry* **2019**.

57.	Villar López, R.; Faza, O. N.; Silva López, C., Dynamic Effects Responsible for High Selectivity in a [3,3] Sigmatropic Rearrangement Featuring a Bispericyclic Transition State. *The Journal of Organic Chemistry* **2017,** *82* (9), 4758-4765.

58.	Patel, A.; Chen, Z.; Yang, Z. Y.; Gutierrez, O.; Liu, H. W.; Houk, K. N.; Singleton, D. A., Dynamically Complex 6+4 and 4+2 Cycloadditions in the Biosynthesis of Spinosyn A. *Journal of the American Chemical Society* **2016,** *138* (11), 3631-3634.

59.	Xu, L.; Doubleday, C. E.; Houk, K. N., Dynamics of Carbene Cycloadditions. *Journal of the American Chemical Society* **2011,** *133* (44), 17848-17854.

60.	Xu, L.; Doubleday, C. E.; Houk, K. N., Dynamics of 1,3-Dipolar Cycloadditions: Energy Partitioning of Reactants and Quantitation of Synchronicity. *Journal of the American Chemical Society* **2010,** *132* (9), 3029-3037.

61.	Black, K.; Liu, P.; Xu, L.; Doubleday, C.; Houk, K. N., Dynamics, transition states, and timing of bond formation in Diels-Alder reactions. *Proceedings of the National Academy of Sciences of the United States of America* **2012,** *109* (32), 12860-12865.

62.   Patel, A.; Chen, Z.; Yang, Z.; Gutiérrez, O.; Liu, H.-w.; Houk, K. N.; Singleton, D. A., Dynamically Complex [6+4] and [4+2] Cycloadditions in the Biosynthesis of Spinosyn A. *Journal of the American Chemical Society* **2016,** *138* (11), 3631-3634.

63.   Chai, J.-D.; Head-Gordon, M., Long-range corrected hybrid density functionals with damped atom-atom dispersion corrections. *PCCP* **2008,** *10* (44), 6615-6620.